Precisely Encoded Barcodes Using Tetrapod CdSe/CdS Quantum Dots with a Large Stokes Shift for Multiplexed Detection

Weijie Wu, Xujiang Yu, Mengyu Gao, Sehrish Gull, Lisong Shen, Weiwei Wang, Li Li, Yue Yin, and Wanwan Li*

A serious obstacle to the construction of high-capacity optical barcodes in suspension array technology is energy transfer, which can prompt unpredictable barcode signals, limited barcode numbers, and the need for an unfeasible number of experimental iterations. This work reports an effective and simple way to eliminate energy transfer in multicolor quantum dots (QDs)-encoded microbeads by incorporating tetrapod CdSe/CdS QDs with a large Stokes shift (about 180 nm). Exploiting this unique feature enables the facile realization of a theoretical 7 × 7-1 barcoding matrix combining two colors and seven intensity levels. As such, microbeads containing tetrapod CdSe/CdS QDs are demonstrated to possess a powerful encoding capacity which allows for precise barcode design. The ability of the Shirasu porous glass membrane emulsification method to easily control microbead size facilitates the establishment of a 3D barcode library of 144 distinguishable barcodes, indicating the enormous potential to enable large-scale multiplexed detection. Moreover, when applied for the multiplexed detection of five common allergens, these barcodes exhibit superior detection performance (limit of detection: 0.01–0.02 IU mL^{-1}) for both spiked and patient serum samples. Therefore, this new coding strategy helps to expand barcoding capacity while simultaneously reducing the technical and economic barriers to the optical encoding of microbeads for high-throughput multiplexed detection.

Dr. W. Wu, X. Yu, M. Gao, S. Gull, Prof. W. Li
State Key Lab of Metal Matrix Composites
School of Materials Science and Engineering
Shanghai Jiao Tong University
800 Dongchuan Road, Shanghai 200240, P. R. China
E-mail: wwli@sjtu.edu.cn
Prof. L. Shen, Dr. W. Wang
Xinhua Hospital Affiliated to Shanghai Jiao Tong
University School of Medicine
Shanghai Jiao Tong University
1665 Kongjiang Road, Shanghai 200092, P. R. China
Prof. L. Li, Dr. Y. Yin
The First People's Hospital Affiliated to Shanghai Jiao Tong
University School of Medicine
Shanghai Jiao Tong University
100 Haining Road, Shanghai 200080, P. R. China

The ORCID identification number(s) for the author(s) of this article can be found under https://doi.org/10.1002/adfm.201906707.

1. Introduction

Suspension array technology (SAT) based on encoded microbeads plays a prominent role in multiplexed detection of analytes within a small, single sample volume, making it widely useful for single-cell analysis, protein profiling, gene analysis, and early disease diagnosis and prognosis.[1–6] Encoded microbeads are a vital component of SAT, as they are endowed with solid supports and tracking codes for the detection of a specific target. Therefore, achieving high-throughput multiplexing detection requires a sufficient number of barcodes.[7–11] Current optical encoding strategies typically combine color and intensity to allow for flexible encoding and high-speed decoding,[7,12–17] is the most prevalent comparing with other many encoding methods such as graphical encoding, physical encoding, chemical encoding, and electronic encoding.[7,13,18] Optical coding strategies generally utilize fluorophores [e.g., organic dyes, quantum dots (QDs)] which emit two or more colors to achieve a greater number of barcodes. However, the spectral overlap among multicolor fluorophores inevitably generates an intractable ensemble fluorescence phenomenon, such as stochastic Förster resonance energy transfer (FRET) and photon re-absorption, resulting in a non-orthogonal fluorescence response.[19–24] Consequently, this limits the number of barcodes and renders the achieved barcode signals difficult to predict or design, even when accurate ratios of fluorophores are incorporated into microbeads.[8,19,20,25] Acquiring a sufficient number of distinguishable barcodes therefore requires considerable experimental iterations, an inaccessible option for many scientists due to the technical and economic entry barriers to constructing a high-capacity multiplexed detection platform.[19]

FRET is a strongly distance-dependent non-radiative energy transfer within a luminescent donor–acceptor pair whose components are in the proximity of approximately 1–10 nm from each other.[23,26,27] Similarly, photon re-absorption is radiative energy transfer in a donor–acceptor pair, wherein a photon emitted by the donor is absorbed by the acceptor.[27] Photon

ADVANCED
SCIENCE NEWS
www.advancedsciencenews.com

ADVANCED
FUNCTIONAL
MATERIALS
www.afm-journal.de

re-absorption is more difficult to eliminate since it can occur at lower concentration than FRET can.[26] The necessary condition for both FRET and photon re-absorption is spectral overlap between the emission spectrum of the donor and the absorbance spectrum of the acceptor. Although FRET is a powerful tool for structure elucidation, inter- and intracellular processes, optical imaging, and medical diagnostics,[27–32] it unfortunately acts as a substantial barrier for the optical encoding of barcodes in SAT. An alternative approach towards achieving precise barcode design is establishing FRET model to predict the fluorescence intensity of barcodes.[19] Notably, the ensemble mFRET (emFRET) model constructed by Juncker et al. afforded quantitative insight into stochastic mFRET cascades to guide barcoding via rational design and fine-tuning of the spectral response.[19] However, the emFRET model still cannot aviod the energy transfer among different fluorescent materials, resulting in relatively limited barcode numbers. Other strategies to overcome experimental difficulties imposed by FRET and photon re-absorption include several methods which are theoretically possible for eliminating these phenomena. This could be realized by controlling the distance between different colors of fluorophores so that it is greater than 10 nm, and by careful selection of fluorophores which exhibit a large Stokes shift as encoding elements to inhibit energy transfer among them and achieve the ideal optical encoding number of barcodes ($N^m - 1$ unique spectral barcodes, for fluorophores with m emission colors at N concentrations).[7,22,33,34] Both the H. Xu and J. Xu groups incorporated single color fluorophores into beads and then generated barcodes by conjugating or mixing beads of different colors together.[22,33] Although this method allowed for barcode design while eliminating FRET and photon re-absorption, it involved a cumbersome preparation process and yielded complicated barcode structures.

Common fluorophores with a large Stokes shift include upconversion nanoparticles (UCNPs),[17,35] doped QDs,[34,36] and QDs with heterostructures,[37–40] among others. The multicolor emission of UCNPs renders the optical crosstalk between barcodes and label dyes difficult to avoid.[7] Although doped QDs exhibit excellent optical properties, their relatively wide full width at half maximum (FWHM) cause the emission and excitation spectra of different QDs to overlap. Furthermore, previous reports have demonstrated that the Stokes shift of QDs can be manipulated via their morphology and composition.[34,39–41] Interestingly, reports of tetrapod QDs indicate that these materials not only have excellent luminescent properties, but also possess a large Stokes shift and narrow FWHM (about 30 nm),[38,42] making them ideal candidates for encoded elements and eliminating energy transfer during barcode encoding. To the best of our knowledge, no report has demonstrated the elimination of FRET and photon re-absorption of optical barcodes by preventing the spectral overlap of different fluorophores.

Herein, we report an effective and simple way to eliminate FRET and photon re-absorption phenomena in multicolor QDs-encoded microbeads by incorporating tetrapod CdSe/CdS QDs with a large Stokes shift. CdSe/CdS tetrapod QDs (tQD650) with a phycoerythrin (PL) peak at 650 nm, a large Stokes shift (about 180 nm), and a narrow FWHM (about 30 nm) were used in combination with CdSe/ZnS intrinsic QDs (iQD525)

with a PL peak at 525 nm as model encoding fluorophores with no spectral overlap. A series of microbeads encoded via the incorporation of different amounts of tQD650 and iQD525 were synthesized using the Shirasu porous glass (SPG) membrane emulsification method. An ideal 7 × 7-1 barcoding matrix was facilely constructed by combining two colors and seven intensity levels. Furthermore, the controllability of microbead size conferred by the SPG membrane emulsification method allowed for the establishment of a 3D barcode library with color, intensity, and diameter as coding elements, which combined to allow for a powerful encoding capacity. Finally, the biodetection abilities of the barcodes were demonstrated via a five-plex multiplexed bioassay wherein the QDs-encoded barcodes were incorporated into a suspension array platform. Five common allergens (milk, artemisia pollen, peanut, house dust mite, and egg white) were detected and experimentally validated in patient serum samples, with the results comparable to those obtained by clinical diagnostic methods. This indicates their great potential for future laboratory research and clinical practice applications in high-throughput multiplexed detection.

2. Results and Discussion

2.1. Energy Transfer Between QDs with Spectral Overlap (Donor Emission Spectrum and Acceptor Absorbance Spectrum) in Solution

The encoding of microbeads with multicolor fluorophores, such as traditional organic dyes or conventional intrinsic QDs, is complicated by the problem of unpredictable barcode signals and limited numbers of barcodes. These problems are ubiquitous and intractable due to the uncertain energy transfer between different fluorophores. As such, energy transfer among different fluorophores in solution, as shown in **Figure 1**, is also inevitable and unpredictable.[26,27] To investigate the energy transfer behavior between different intrinsic QDs with spectral overlap (specifically, an overlap of the emission spectrum of donor and the acceptor absorbance spectrum) in solution, we selected two common QDs with strong spectral overlap, namely CdSe/ZnS intrinsic QDs which exhibit a PL peak at 525 nm (iQD525) and CdSe/ZnS intrinsic QDs which exhibit a PL peak at 655 nm (iQD655). Transmission electron microscope (TEM) images show that the iQD525 and iQD655 have uniform size and good crystal structure (see Figure 1a,b). As shown in Figure 1c, the Stokes shift of iQD525 and iQD655 is 23 and 15 nm, respectively. UV–vis absorption and emission spectra of the QDs (see Figure 1c) demonstrate that the emission spectrum of the donor (iQD525) significantly overlaps with the absorption spectrum of the acceptor (iQD655, see Figure 1d). Thus, the strong spectral overlap and small Stokes shift of iQD655 render energy transfer inevitable. Changes to the fluorescence intensities of iQD525 and iQD655 before and after mixing in hexane at different concentrations are illustrated in Figure 1e,f, and Figure S1 in the Supporting Information. Mixing in hexane prompts a sharp decrease (27%–45%) to the fluorescence intensity of iQD525 and a considerable increase (35%–45%) to that of iQD655 (see Table S1, Supporting Information). This significant variations in fluorescence intensity
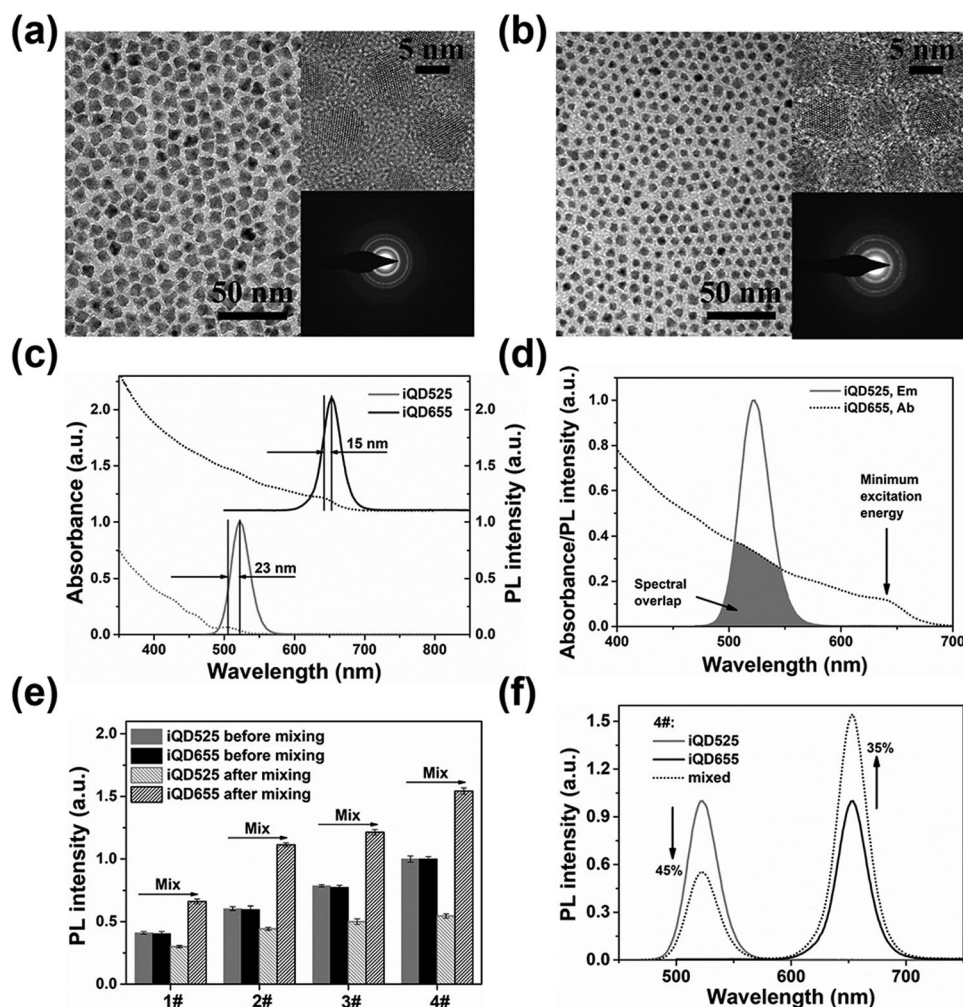
Figure 1. Energy transfer between iQD525 and iQD655 with spectral overlap in solution. TEM images of a) iQD525 and b) iQD655. TEM image inserts represent the corresponding high-resolution transmission electron microscopy (HRTEM, top right) and selected area electron diffraction (SAED) patterns (bottom right). c) UV–vis absorption and emission spectra of iQD525 and iQD655. d) Spectral overlap between the emission spectrum of iQD525 and the absorption spectrum of iQD655. e) Variation of fluorescence intensity of iQD525 and iQD655 before and after mixing in hexane at different concentrations (4, 6, 8, and 10 µg mL^{-1}). f) Fluorescence spectra of single-color QDs and mixed QDs in hexane at the fourth concentration level (10 µg mL^{-1}). Green and blue solid lines represent individual iQD525 and iQD655 in hexane, respectively; the black dotted line represents mixed QDs (iQD525 and iQD655) in hexane.

further confirm the existence of energy transfer, such as FRET and photon re-absorption, between the QDs. This energy transfer is made possible by the small Stokes shift and the spectral overlap of iQD525 and iQD655 in solution. Such energy transfer can be expected to be even more pronounced and complicated among multicolor fluorophores, due to its randomness and unpredictability.[28,43,44]

2.2. Energy Transfer Between QDs Without Spectral Overlap in Solution

Since the small Stokes shift of intrinsic QDs is the main contributing factor to spectral overlap, it is anticipated that utilizing QDs with enlarged Stokes shift may be an effective way to inhibit energy transfer. For this work, we selected CdSe/CdS tetrapod QDs to serve as model QDs with a large

Stokes shift, which can be realized by controlling the CdSe core and tetrapod CdS shell heterostructure. This heterostructure confines the holes to the CdSe core while the electrons move freely throughout the entire particle, resulting in a large Stokes shift.[37,38,45] Synthesis of CdSe/CdS tetrapod QDs was accomplished by the seeded growth method (see Experimental Section for details). To summarize, zinc-blende CdSe (zb-CdSe) core QDs were first synthesized, and then wurtzite CdS (w-CdS) was nucleated and grown from the zb-CdSe facets. The emission wavelengths of the CdSe/CdS tetrapod QDs were flexibly regulated by the diameter and concentration of zb-CdSe core QDs, as well as by the temperature and reaction time allowed for shell growth (see **Figure 2**a,b). Three representative CdSe/CdS tetrapod QDs with large Stokes shift emitted at 615, 632, and 650 nm were synthesized by controlling only the shell growth reaction time, with QDs samples corresponding to growth times of 10, 15, and 20 min, respectively.
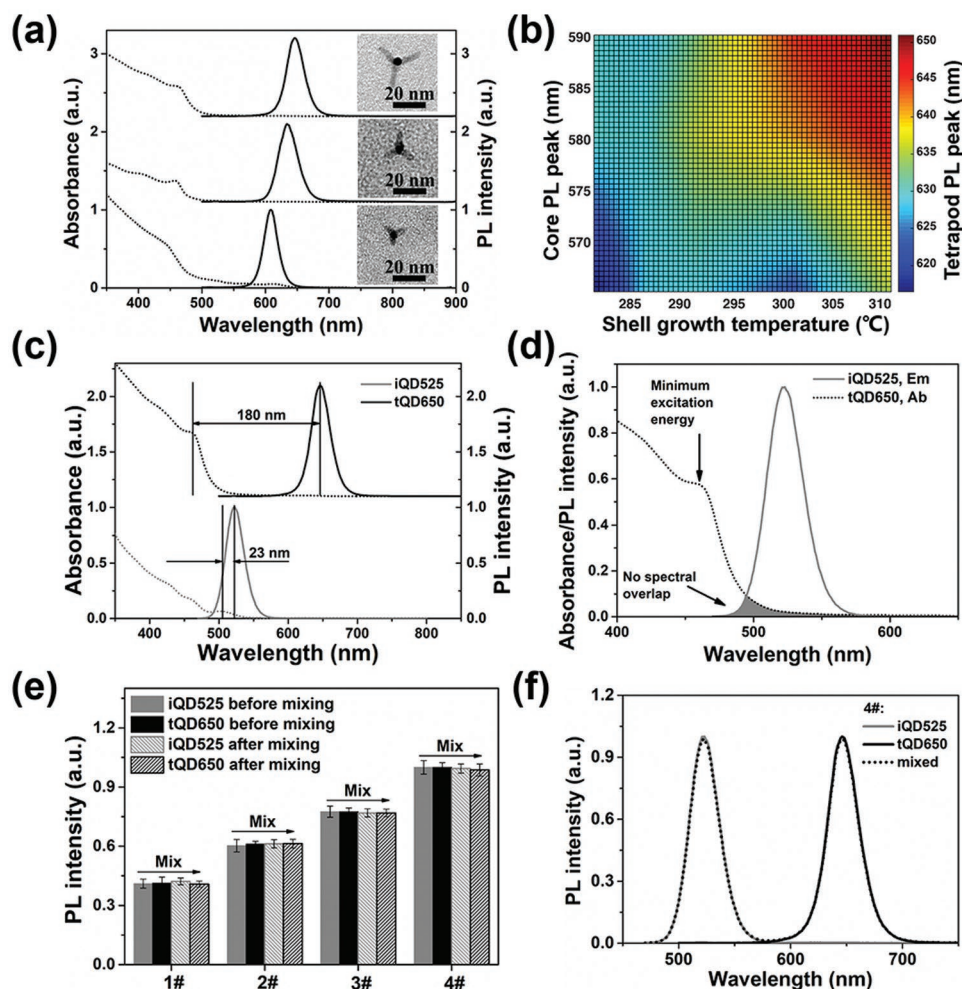
**ADVANCED
SCIENCE NEWS**
www.advancedsciencenews.com

**ADVANCED
FUNCTIONAL
MATERIALS**
www.afm-journal.de

Figure 2. Energy transfer (no FRET or photon re-absorption) between iQD525 and tQD650 without spectral overlap in solution. a) Absorbance and emission spectra of representative CdSe/CdS tetrapod QDs. The inserts display the corresponding TEM images. b) PL peaks of the CdSe/CdS tetrapod QDs as a function of zb-CdSe core QDs diameter and shell growth temperature. c) UV–vis absorption and emission spectra of iQD525 and tQD650. d) No spectral overlap between iQD525 and tQD650 occurs above the minimum excitation energy. e) Variation of fluorescence intensity of iQD525 and tQD650 before and after mixing in hexane at different concentrations (4, 6, 8, and 10 µg mL^{-1}). f) Fluorescence spectrum of single-color QDs and mixed QDs in hexane at the 4th concentration level (10 µg mL^{-1}). Solid lines represent individual iQD525 and tQD650 in hexane, respectively; the black dotted line represents mixed QDs (iQD525 and tQD650) in hexane.

We found that with increasing reaction time, the lengths of tetrapod QDs increase and the emission peaks experience a significant redshift (see Figure 2a). Moreover, a series of orthogonal experiments were carried out to study how tetrapod QDs synthesis is affected by adjusting the emission peak of core QDs (from 565 to 590 nm) and the shell growth reaction temperature (from 280 °C to 310 °C) while other reaction parameters are held constant. On the whole, both larger core QDs diameter and higher shell growth temperature produce tetrapod QDs with emissions of longer wavelengths (see Figure 2b). Accordingly, it is possible to synthesize tunable emission wavelengths of CdSe/CdS tetrapod QDs (from 615 to 650 nm) with a large Stokes shift (see Figure 2a,b).

Consideration of the detection channels (Violet 660, 660/20 bandpass, BP) of flow cytometry led to the selection of CdSe/CdS tetrapod QDs, which exhibit a PL peak at 650 nm and a large Stokes shift (180 nm) and were designated tQD650,

together with iQD525 to serve as model materials for investigating energy transfer (see Experimental Section for details and Figure 2c, and Figures S2 and S3, Supporting Information). Figure 2c displays these materials' UV–vis absorption and emission spectra, which clearly indicate that no spectral overlap occurs between the emission spectrum of iQD525 and the absorption spectrum of tQD650, especially above the minimum excitation energy of tQD650 (see Figure 2d). This, in combination with the large Stokes shift of tQD650, renders FRET and photon re-absorption theoretically implausible between these two QDs. Solutions of varying iQD525 and tQD650 concentrations do not exhibit varied fluorescence intensity, indicating that no energy transfer takes place (see Figure 2e, f, and Figure S4, Supporting Information). Therefore, our strategy of exploiting tetrapod QDs with large Stokes shift to inhibit spectral overlap and eliminate energy transfer in different QDs is simple and effective in solution.
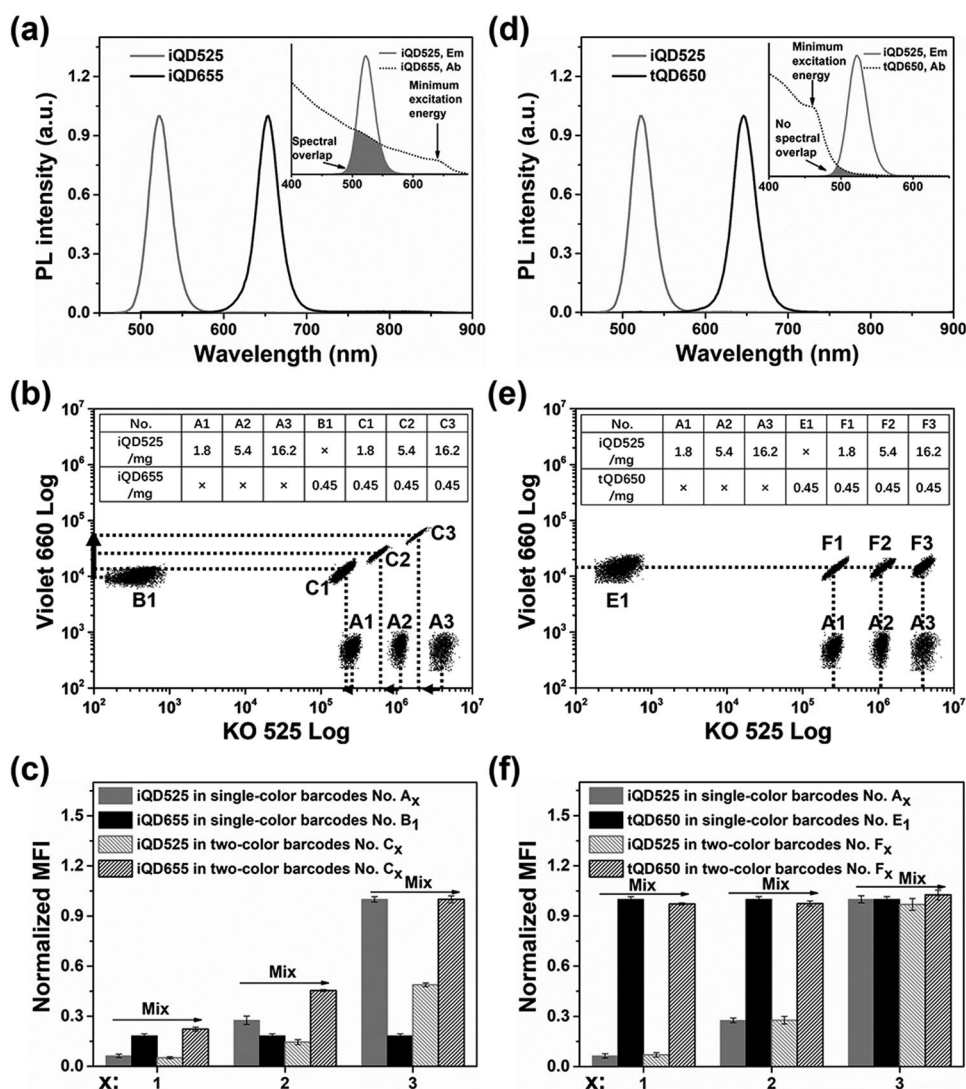
Figure 3. Energy transfer between QDs with/without spectral overlap inside microbeads. a–c) iQD525 and iQD655 with spectral overlap in microbeads. d–f) iQD525 and tQD650 without spectral overlap in microbeads. a, d) The emission spectra of different QDs. The insert shows the spectral overlap between the donor emission spectrum and the acceptor absorption spectrum. b,e) Relative positions of QDs-encoded microbeads with single- and two-color QDs. Groups A_x, B_x, and E_x represent beads containing only iQD525, iQD655, and tQD650, respectively; and groups C_x and F_x represent microbeads with mixtures of different types of QDs. The table inserts provide the microbead compositions. c, f) Variation of fluorescence intensity of iQD525, iQD655, and tQD650 in single- and multicolor-QDs-encoded microbeads.

2.3. Energy Transfer Between QDs Inside Microbeads

As previously discussed, QDs with spectral overlap exhibit substantial energy transfer upon mixing in solution. Therefore, to improve the suitability of the QDs for encoding applications, it is important to investigate the energy transfer behavior inside microbeads. QDs-encoded microbeads were synthesized via the SPG membrane emulsification method using an SPG membrane with a pore size of 4.9 µm (see Experimental Section for details).[46,47] iQD525 and iQD655 were incorporated into microbeads (see **Figure 3**a), with the iQD655 content fixed at 0.45 mg and the iQD525 content adjusted to 1.8, 5.4, or 16.2 mg. The table inserted in Figure 3b provides the QDs composition of each barcode. Measurements of the fluorescence intensity of iQD525 and iQD655 were conducted via flow

cytometry detection channels of KO 525 (525/40 BP) and Violet 660 (660/20 BP), respectively, with a 405 nm laser serving as the excitation source.

Increasing iQD525 content (from 1.8 to 5.4 to 16.2 mg) prompts a notable shift leftwards and upwards to the barcoding signal positions of the two-color encoded microbeads compared to those of the corresponding single-color encoded microbeads (see Figure 3b). As such, with increasing iQD525 content the fluorescence intensity of iQD525 in two-color encoded microbeads decreases sharply (1–2 times), while that of iQD655 increases dramatically (1–5 times, see Figure 3c and Table S2, Supporting Information). That is to say, higher QDs content within the microbeads promotes stronger energy transfer in multicolor microbeads (see Figure 3c and Table S2, Supporting Information). Therefore, energy transfer also occurs

**ADVANCED
SCIENCE NEWS**
www.advancedsciencenews.com

**ADVANCED
FUNCTIONAL
MATERIALS**
www.afm-journal.de

in microbeads containing QDs with spectral overlap, and is in fact even more acute than in corresponding solutions of QDs, which may result from the considerable shrinkage of microbeads compared to their original emulsion droplets (see Tables S1 and S2, Supporting Information). More specifically, since the solidification of microbeads involves the evaporation of organic solvent from the emulsion droplet and a simultaneous decrease to the volume of microbeads (about 12 times), the distance between QDs is shorter in the microbeads than in the emulsion droplets (see Figure S5, Supporting Information). This closer proximity results in stronger distance-dependent FRET in the microbeads. This makes the prediction of a two-color barcoding signal based on the position of single-color barcodes challenging. Energy transfer which is already blatant during the preparation of two-color barcodes could be expected to be even more so in multicolor barcoding due to the greater degree of energy transfer randomness and complexity to yield various fluorophores.[19,20] Hence, multicolor barcodes signals are more unpredictable due to the non-orthogonal fluorescence response, giving rise to numerous experimental iterations. This greatly increases the technical and economic entry barriers to constructing a high-capacity multiplexed platform.[19,20,33]

Our simple strategy effectively eliminates energy transfer between QDs without spectral overlap in solution, which could be expected to enable precise multicolor barcode design. However, it is first essential to examine how QDs with no spectral overlap undergo energy transfer in microbeads. We incorporated iQD525 and tQD650 into microbeads (see Figure 3d) whose tQD650 content was fixed at 0.45 mg. Figure 3e displays the barcoding signal relative positions of single- and two-color encoded microbeads. Increasing iQD525 content does not prompt any leftwards or upwards shift of the signal relative positions of the two-color encoded microbeads compared to those of the corresponding single-color encoded microbeads. As shown in Figure 3f, the fluorescence intensity of microbeads containing iQD525 and tQD650 exhibits no difference whether the corresponding microbeads are two- or single-color encoded. Overall, these phenomena directly demonstrate that FRET and photon re-absorption can be effectively avoided by incorporating different QDs with no spectral overlap during barcode generation via multicolor QDs encoding. Therefore, the initial determination of single-color barcoding signals based on the ratio of incorporated QDs can serve as a springboard from which the multicolor barcoding signal can be precisely predicted according to the position of single-color barcodes.

2.4. Precise Coding and Construction of QDs-Encoded Barcode Library

The aforementioned results demonstrate that energy transfer can be effectively eliminated by mixtures of QDs with no spectral overlap both in solution and microbeads. This indicates the power of this simple method to guide the construction of a barcode library. Moreover, this allows for precise barcode design, eliminating the sources of the substantial barriers to constructing a high-capacity multiplexed platform, such as unpredictable barcode signals, limited numbers of barcodes, and the considerable number of experimental iterations required. For

this set of experiments, the barcode preparation process is the same as previously described. 7 μm of QDs-encoded microbeads were generated via the SPG membrane emulsification method using a SPG membrane with a pore size of 4.9 μm (see Experimental Section for details).[46,47] Scanning electron microscopy (SEM) images reveal highly uniform microbeads with smooth surfaces and a coefficient of variation (CV%) of about 8% (see **Figure 4**a and Figure S6, Supporting Information). A series of luminescence images captured via laser scanning confocal microscopy (LSCM) depict three representative microbeads incorporated with iQD525, tQD650, and a mixture of both QDs, respectively (see Figure S7, Supporting Information). Each of the microbeads exhibits high fluorescence intensity and fluorescence uniformity. Moreover, the as-prepared QDs-encoded microbeads also display excellent fluorescence stability across a range of different, even extreme, conditions (see Figures S8 and S9, Supporting Information), indicating their suitability for further application in biomedical detection.

A 2D barcodes library combining color and intensity was first constructed by incorporating iQD525 and tQD650 at seven different intensity levels (0–6) to facilely construct an ideal 7 × 7-1 barcoding matrix (see Figure 4d). Seven distinguishable single-color barcodes were first identified by incorporating accurate ratios iQD525 and tQD650, respectively. The signal positions of the single-color barcodes then informed the precise design of corresponding two-color barcodes. We used a flow cytometry to decode the barcodes due to its rapid signal reading and high-throughput abilities. During the decoding process, microbeads were individually excited by 405 nm laser in a Beckman CytoFLEX flow cytometry, and the fluorescence signal of each microbead was collected in KO 525 (525/40 BP) and Violet 660 (660/20 BP) detection channels. The measured barcode signal is shown in Figure 4d. The barcode is designated GyRz, which represents iQD525 (G) at a relative intensity level of y, and tQD650 (R) at a relative intensity level of z. For example, barcodes corresponding to pure iQD525 barcodes are G1R0, G2R0, G3R0, G4R0, G5R0, and G6R0. Similarly, G3R5 refers to a barcode containing iQD525 at a relative intensity level of 3 and tQD650 at a relative intensity level of 5. Figure 4e,f shows the corresponding histograms for QDs-encoded barcodes as measured by the 525/40 BP and 660/20 BP detection channels, respectively, which are in good agreement with Figure 4d. As expected, no energy transfer occurs during the barcoding process, and the barcode signal is precisely designable via incorporation of particular ratios of QDs into the microbeads.

Finally, as a proof of concept, an ideal 7 × 7-1 barcoding matrix consisting of two colors and seven intensity levels was facilely generated and used to achieve precise barcode design. Exploiting the ability of the SPG membrane emulsification method to control microbead size facilitated the establishment of a 3D barcode library combining color, intensity, and diameter as coding elements. QDs were incorporated into microbeads of three different diameters (7, 11, and 16 μm), which were generated by simply changing the SPG membrane pore size (4.9, 9, and 13 μm, respectively). SEM images of 11 and 16 μm microbeads reveal high homogeneity (see Figure 4b,c). A 3D barcode library was then constructed from microbeads of varied diameters containing iQD525 and tQD650. When diameter serves as the third encoding element, the barcode is designated X-GyRz, where X represents
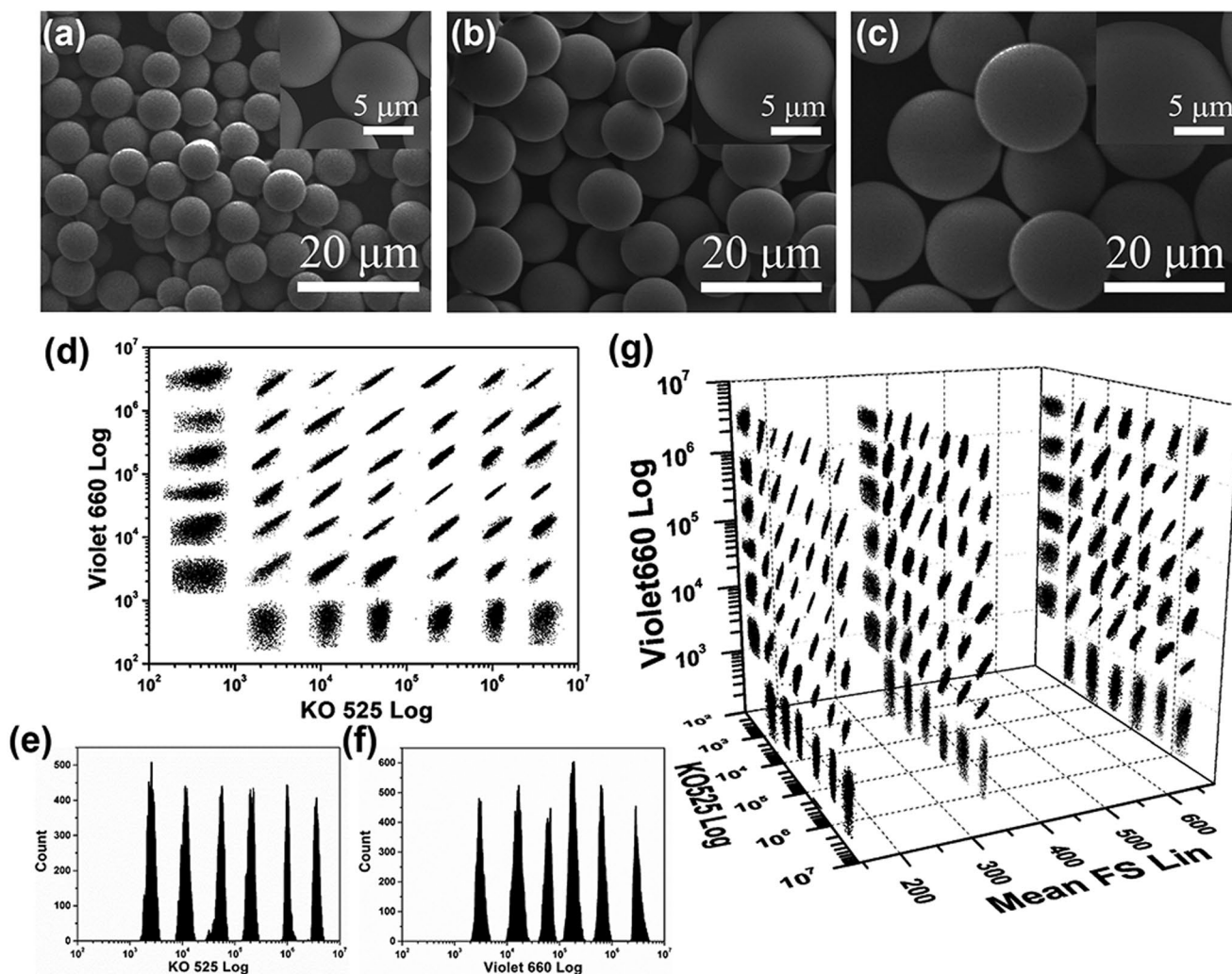
ADVANCED
SCIENCE NEWS
www.advancedsciencenews.com

ADVANCED
FUNCTIONAL
MATERIALS
www.afm-journal.de

Figure 4. Construction of QDs-encoded barcodes library. a–c) SEM images of QDs-encoded microbeads with different diameters produced by SPG membranes of different pore sizes: a) 4.9 μm, b) 9 μm, and c)13 μm. d) 2D QDs-encoded barcodes library (7 × 7-1) based on the emission color and fluorescence intensity of iQD525 and tQD650 at seven concentration levels as measured via flow cytometry. Histogram for QDs-encoded barcodes as measured by e) 525/40 BP and f) 660/20 BP detection channels. g) 3D barcodes library containing 144 QDs-encoded microbeads which vary according to size (7, 11, and 16 μm) as well as the color and intensity of iQD525 and tQD650. Mean FS value and barcode size are positively correlated.

the diameter. For example, 11-G4R2 indicates a barcode with a diameter of 11 μm containing iQD525 and tQD650 at relative intensity levels of 4 and 2, respectively. A 7 × 7-1 barcoding matrix was generated for each of the three differently sized microbeads to yield a 3D barcodes library of 144 distinguishable barcodes as measured by flow cytometry (Figure 4g). In summary, our new encoding strategy successfully guided us to construct a large barcode library via precise design, which was achieved through the incorporation of particular ratios of different fluorophores. In this way, it is possible to eliminate FRET and photon re-absorption phenomena, expand the barcoding capacity, and reduce technical and economic entry barriers to the optical encoding of microbeads for high-throughput multiplexed detection.

2.5. Multiplexed Allergens Detection

After successfully constructing a series of distinguishable QDs-encoded microbeads, we further demonstrated the practical

applicability of the microbeads by performing five-plex multiplexed detection of five common allergens, namely milk, artemisia pollen, peanut, house dust mite, and egg white. Such multiplexed detection was carried out in a suspension array platform using QDs-encoded microbeads with the coding addresses 7-G2R2, 7-G4R0, 11-G3R5, 11-G0R2 and 16-G2R6, respectively. During this multiplexed detection of allergens, the selected barcodes served as solid supports by immobilizing allergen antigens in each of the five analytes. The detection targets were specific-IgE antibodies of allergens in the samples, which bound with corresponding allergen antigens on the surface of microbeads. Finally, goat anti-human IgE secondary antibody labeled with PL was reacted with the mixtures. For each immunoassay, about 5000 size-gated microbeads were analyzed and decoded by mapping the fluorescence profiles measured by the 525/40 BP and 660/20 BP detection channels of the flow cytometry. The median fluorescence intensity (MFI) of PL (peak at ≈580 nm), which is directly related to the concentration of the corresponding target,
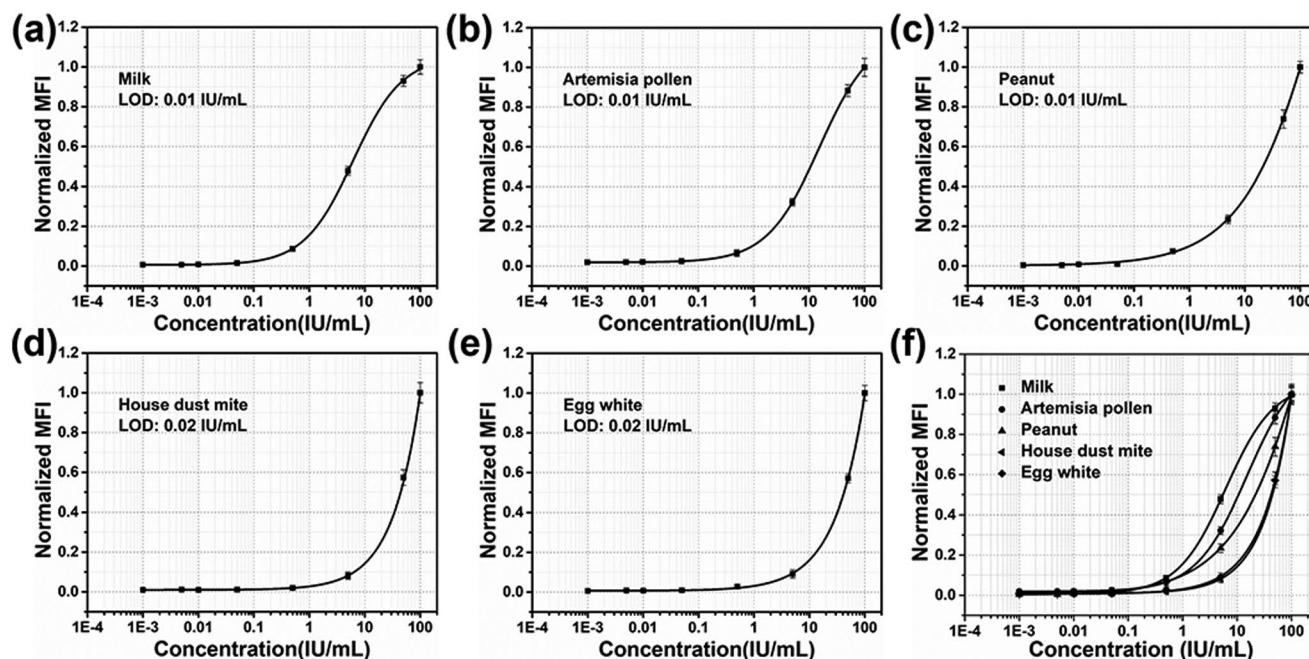
Figure 5. Standard curves for detection of a–e) milk, artemisia pollen, peanut, house dust mite, and egg white in five-plex allergens assay.

was measured by the 585/42 BP detection channel. The results of the five-plex allergens tests of the spiked samples are shown in **Figure 5**, which indicates good linearity of the fitting standard curve between target concentration and normalized MFI of PL for each analyte, as well as excellent detection performance for microbeads of varying sizes and QDs contents (limit of detection, LOD: 0.01–0.02 IU mL^{-1}). For comparison, the LOD of ImmunoCAP, the gold-standard clinical method for quantitative allergen diagnosis, is about 0.1 IU mL^{-1}, which is 1 order of magnitude higher than our detection results. Therefore, encoding barcodes by microbead diameter, color, and intensity is a feasible method for practical application.

To validate its efficacy in clinical practice, we tested 10 cases of serum samples from healthy people and allergic patients using the multiplexed platform. All serum samples were collected and simultaneously detected using the ImmunoCAP method, which was carried out at the First People's Hospital affiliated with Shanghai Jiao Tong University School of Medicine. A procedure similar to that used to test the spiked samples was also used for five-plex allergens detection of patient serum samples, the results of which are depicted in Figure S10 in the Supporting Information. Our results are highly consistent with those obtained by clinical gold-standard method of ImmunoCAP. In summary, compared to clinical diagnostic methods our barcode-based multiplexed detection platform exhibits excellent performance in the detection of spiked samples and patient serum samples.

3. Conclusion

In summary, we report an effective and simple way to eliminate energy transfer in multicolor QDs-encoded microbeads

by incorporating tetrapod CdSe/CdS QDs with large Stokes shift. Enforcing such a large Stokes shift (about 180 nm) in these tetrapod CdSe/CdS QDs, which exhibit an emission peak at 650 nm, enables the efficient inhibition of spectral overlap between the absorption spectrum of tQD650 and emission spectrum of iQD525. We therefore applied this strategy to guide the generation of multicolor QDs-encoded microbeads via the SPG membrane emulsification method by incorporating particular ratios of iQD525 and tQD650, which have no spectral overlap. This allowed us to eliminate energy transfer and spearhead an innovative approach to precise barcode design by constructing an ideal 7 × 7-1 barcoding matrix combining two colors and seven intensity levels. Since the SPG membrane emulsification method also makes it possible to control microbead size, we established a 3D barcode library combining color, intensity, and diameter as coding elements to yield 144 distinguishable barcodes, demonstrating the powerful encoding capacity of our encoding strategy and indicating its promising potential for large-scale multiplexed detection. Moreover, the QDs-encoded barcodes exhibited good performance in the multiplexed detection of five common allergens (LOD: 0.01–0.02 IU mL^{-1}). Our proof-of-concept work imparts greater accessibility to the construction of a high-capacity multiplexed platform, which has been heretofore marked by reducing substantial technical and economic barriers such as unpredictable barcodes signals, limited barcode numbers, and the need for considerable experimental iterations. Furthermore, we hope that the results presented herein will contribute towards a general solution to solve energy transfer problems in other applications using multicolor fluorophore mixtures. It is also need to note that suspension array based on encoded microspheres will be more powerful and robust if we can further improve non-specific biofouling suppression, directional immobilization of biomolecules and develop "point-of-care" diagnostic platforms.

ADVANCED
SCIENCE NEWS
www.advancedsciencenews.com

ADVANCED
FUNCTIONAL
MATERIALS
www.afm-journal.de

Supporting Information

Acknowledgements

Conflict of Interest

The authors declare no conflict of interest.

Keywords

[1] R. Wilson, A. R. Cossins, D. G. Spiller, *Angew. Chem. Int. Ed.* **2006**, *45*, 6104.

[2] J. Kim, M. J. Biondi, J. J. Feld, W. C. Chan, *ACS Nano* **2016**, *10*, 4742.

[3] Y. Leng, W. Wu, L. Li, K. Lin, K. Sun, X. Chen, W. Li, *Adv. Funct. Mater.* **2016**, *26*, 7581.

[4] Y. Lu, J. Lu, J. Zhao, J. Cusido, F. M. Raymo, J. Yuan, S. Yang, R. C. Leif, Y. Huo, J. A. Piper, J. Paul Robinson, E. M. Goldys, D. Jin, *Nat. Commun.* **2014**, *5*, 3741.

[5] S. A. Dunbar, *Clin. Chim. Acta* **2006**, *363*, 71.

[6] C. Ji, P. Jiang, X. Ye, M. Chang, F. Liu, Y. Shen, D. Chen, L. Nie, *Sci. Adv. Mater.* **2019**, *11*, 680.

[7] Y. Leng, K. Sun, X. Chen, W. Li, *Chem. Soc. Rev.* **2015**, *44*, 5552.

[8] F. Hu, C. Zeng, R. Long, Y. Miao, L. Wei, Q. Xu, W. Min, *Nat. Methods* **2018**, *15*, 194.

[9] Y. Lu, J. Zhao, R. Zhang, Y. Liu, D. Liu, E. M. Goldys, X. Yang, P. Xi, A. Sunna, J. Lu, Y. Shi, R. C. Leif, Y. Huo, J. Shen, J. A. Piper, J. P. Robinson, D. Jin, *Nat. Photonics* **2014**, *8*, 32.

[10] V. V. Krishnan, S. R. Selvan, N. Parameswaran, N. Venkateswaran, P. A. Luciw, K. S. Venkateswaran, *J. Immunol. Methods* **2018**, *461*, 1.

[11] Y. Wang, L. Shang, F. Bian, X. Zhang, S. Wang, M. Zhou, Y. Zhao, *Small* **2019**, *15*, 1900056.

[12] M. Han, X. Gao, J. Z. Su, S. Nie, *Nat. Biotechnol.* **2001**, *19*, 631.

[13] Y. Xu, H. Wang, B. Chen, H. Liu, Y. Zhao, *Sci. China Mater.* **2019**, *62*, 289.

[14] D. S. Z. Zhang, Y. Jiang, H. Yang, Y. Zhu, S. Zhang, Y. Zhu, D. Wei, Y. Lin, P. Wang, Q. Fu, *Adv. Funct. Mater.* **2016**, *26*, 6146.

[15] N. Martino, S. J. Kwok, A. C. Liapis, S. Forward, H. Jang, H. Kim, S. J. Wu, J. Wu, P. H. Dannenberg, S. Jang, *Nat. Photonics* **2019**, *13*, 720.

[16] C. Chen, P. Zhang, G. Gao, D. Gao, Y. Yang, H. Liu, Y. Wang, P. Gong, L. Cai, *Adv. Mater.* **2014**, *26*, 6313.

[17] L. Zhou, Y. Fan, R. Wang, X. Li, L. Fan, F. Zhang, *Angew. Chem. Int. Ed.* **2018**, *57*, 12824.

[18] K. Zheng, C. Chen, X. Chen, M. Xu, L. Chen, Y. Hu, Y. Bai, B. Liu, C. Yan, H. Wang, J. Li, *Biosens. Bioelectron.* **2019**, *132*, 47.

[19] M. Dagher, M. Kleinman, A. Ng, D. Juncker, *Nat. Nanotechnol.* **2018**, *13*, 925.

[20] S. Fournier-Bidoz, T. L. Jennings, J. M. Klostranec, W. Fung, A. Rhee, D. Li, W. C. Chan, *Angew. Chem. Int. Ed.* **2008**, *47*, 5577.

[21] L. Wang, W. Tan, *Nano Lett.* **2006**, *6*, 84.

[22] S. Lu, D. S. Zhang, D. Wei, Y. Lin, S. Zhang, H. He, X. Wei, H. Gu, H. Xu, *Chem. Mater.* **2017**, *29*, 10398.

[23] C. Chen, L. Ao, Y. T. Wu, V. Cifliku, M. Cardoso Dos Santos, E. Bourrier, M. Delbianco, D. Parker, J. M. Zwier, L. Huang, N. Hildebrandt, *Angew. Chem. Int. Ed.* **2018**, *57*, 13686.

[24] S. V. Vaidya, A. Couzis, C. Maldarelli, *Langmuir* **2015**, *31*, 3167.

[25] J. Stuchlý, V. Kanderová, K. Fišer, D. Černá, A. Holm, W. Wu, O. Hrušák, F. Lund-Johansen, T. Kalina, *Cytometry, Part A* **2012**, *81A*, 120.

[26] J. R. Lakowicz, *Principles of Fluorescence Spectroscopy*, Springer Science & Business Media, Berlin, Germany **2013**.

[27] I. L. Medintz, N. Hildebrandt, *FRET-Förster Resonance Energy Transfer: from Theory to Applications*, John Wiley & Sons, Oboken, NJ **2013**.

[28] N. Hildebrandt, C. M. Spillmann, W. R. Algar, T. Pons, M. H. Stewart, E. Oh, K. Susumu, S. A. Diaz, J. B. Delehanty, I. L. Medintz, *Chem. Rev.* **2017**, *117*, 536.

[29] V. Gubala, L. F. Harris, A. J. Ricco, M. X. Tan, D. E. Williams, *Anal. Chem.* **2012**, *84*, 487.

[30] X. Fang, Y. Zheng, Y. Duan, Y. Liu, W. Zhong, *Anal. Chem.* **2019**, *91*, 482.

[31] J. Guo, X. Qiu, C. Mingoes, J. R. Deschamps, K. Susumu, I. L. Medintz, N. Hildebrandt, *ACS Nano* **2019**, *13*, 505.

[32] N. Melnychuk, A. S. Klymchenko, *J. Am. Chem. Soc.* **2018**, *140*, 10856.

[33] Y. Chen, P. Dong, J. Xu, G. Luo, *Langmuir* **2014**, *30*, 8538.

[34] X. Wang, X. Yan, W. Li, K. Sun, *Adv. Mater.* **2012**, *24*, 2742.

[35] S. Wen, J. Zhou, K. Zheng, A. Bednarkiewicz, X. Liu, D. Jin, *Nat. Commun.* **2018**, *9*, 2415.

[36] M. Makkar, R. Viswanatha, *RSC Adv.* **2018**, *8*, 22103.

[37] D. V. Talapin, J. H. Nelson, E. V. Shevchenko, S. Aloni, B. Sadtler, A. P. Alivisatos, *Nano Lett.* **2007**, *7*, 2951.

[38] K. Manthiram, B. J. Beberwyck, D. V. Talapin, A. P. Alivisatos, *J. Vis. Exp.* **2013**, *82*, e50731.

[39] S. Deka, A. Quarta, M. G. Lupo, A. Falqui, S. Boninelli, C. Giannini, G. Morello, M. De Giorgi, G. Lanzani, C. Spinella, *J. Am. Chem. Soc.* **2009**, *131*, 2948.

[40] J. Jung, C. H. Lin, Y. J. Yoon, S. T. Malak, Y. Zhai, E. L. Thomas, V. Vardeny, V. V. Tsukruk, Z. Lin, *Angew. Chem. Int. Ed.* **2016**, *55*, 5071.

[41] W. Zheng, Z. Wang, J. van Tol, N. S. Dalal, G. F. Strouse, *Nano Lett.* **2012**, *12*, 3132.

[42] L. Manna, D. J. Milliron, A. Meisel, E. C. Scher, A. P. Alivisatos, *Nat. Mater.* **2003**, *2*, 382.

[43] C. M. Spillmann, S. Buckhout-White, E. Oh, E. R. Goldman, M. G. Ancona, I. L. Medintz, *Chem. Commun.* **2014**, *50*, 7246.

[44] S. Hohng, S. Lee, J. Lee, M. H. Jo, *Chem. Soc. Rev.* **2014**, *43*, 1007.

[45] J. Huang, M. V. Kovalenko, D. V. Talapin, *J. Am. Chem. Soc.* **2010**, *132*, 15866.

[46] G. Wang, Y. K. Leng, H. J. Dou, L. Wang, W. W. Li, X. B. Wang, K. Sun, L. S. Shen, X. L. Yuan, J. Y. Li, K. Sun, J. S. Han, H. S. Xiao, Y. Li, *ACS Nano* **2013**, *7*, 471.

[47] X. Wang, G. Wang, W. Li, B. Zhao, B. Xing, Y. Leng, H. Dou, K. Sun, L. Shen, X. Yuan, J. Li, K. Sun, J. Han, H. Xiao, Y. Li, P. Huang, X. Chen, *Small* **2013**, *9*, 3327.